Earthquakes and Structures, *Vol. 16, No. 4 (2019) 437-453*
DOI: https://doi.org/10.12989/eas.2019.16.4.437

Optimum design of viscous dampers to prevent pounding of adjacent structures

Turan Karabork[1a] and Ersin Aydin[*2,]

[1]*Aksaray University, Engineering Faculty, Department of Civil Engineering, Aksaray, Turkey*
[2]*Niğde Ömer Halisdemir University, Engineering Faculty, Department of Civil Engineering, Nigde, Turkey*

(Received January 24, 2019, Revised March 7, 2019, Accepted March 15, 2019)

Abstract. This study investigates a new optimal placement method for viscous dampers between structures in order to prevent pounding of adjacent structures with different dynamic characteristics under earthquake effects. A relative displacement spectrum is developed in two single degree of freedom system to reveal the critical period ratios for the most risky scenario of collision using El Centro earthquake record (NS). Three different types of viscous damper design, which are classical, stair and X-diagonal model, are considered to prevent pounding on two adjacent building models. The objective function is minimized under the upper and lower limits of the damping coefficient of the damper and a target modal damping ratio. A new algorithm including time history analyses and numerical optimization methods is proposed to find the optimal dampers placement. The proposed design method is tested on two 12-storey adjacent building models. The effects of the type of damper placement on structural models, the critical period ratios of adjacent structures, the permissible relative displacement limit, the mode behavior and the upper limit of damper are investigated in detail. The results of the analyzes show that the proposed method can be used as an effective means of finding the optimum amount and location of the dampers and eliminating the risk of pounding.

Keywords: pounding, collision; relative displacement spectrum; viscous dampers; adjacent structures; earthquake resistant structures

1. Introduction

In the last century, commercial areas especially in city centers are very prevalent, so adjacent structures are frequently preferred. These structures are usually constructed without any structural connections. Non-phase response of neighbor structures gives rise to pounding or hammering phenomena during strong earthquakes or winds. Dissimilarity between dynamic parameters of structures such as height, stiffness, mass and damping bring about out-of-phase oscillation. The nature of pounding is very complicated and it reveals a civil engineering issue that is uneasy to solve. Collision of adjacent buildings with huge masses provides high stroke effects that can be unpredicted. Pounding or collision at adjacent structures results in the critical damage and partially or completely collapse of the structure in many strong earthquakes (Chouw and Hao 2012, Schexnayder *et al.* 2014).

The simplest way to avoid from pounding is to build one away from the other. In order to prevent the collision, different design codes in different countries in the world have identified sufficient gap amounts and design principles between two adjacent structures (Rajaram and Kumar 2015).

These gaps between the buildings may not be sufficient during severe earthquakes, especially in the case of out-of-phase vibrations of structures. The optimal conditions were provided based on an energy concept in order to solve the gap between adjacent structures under lateral forces (Stavroulakis and Abdalla 1991). Jeng *et al.* (1992) investigated the "Spectral Difference Method and Double Difference Combination" rule based on random vibration theory to calculate the demand gap and avoiding collision. Damage reports has published that collision appeared in approximately 330 structural failure or heavily damaged building; just about 15% of adjacent buildings, collision was the first cause of the failure and heavy damage (Anagnostopoulos 1995). An investigation on building failure in terms of collision of neighbor buildings has been presented (Penzien 1997). The minimum earthquake gap was calculated and proposed a method based on the pseudo energy radius to prevent collision (Valles-Mattox 1996). A statistical approximation to calculate proper gap of adjacent structures in terms of random vibration theory to avoid collision was presented by Lin (1997). Lin and Weng (2001) examined pounding phenomena at the top floor of a low-rise building and evaluated the collision possibilities of neighbor structures kept apart by a specific distance to avoid collision. Vibration experiments were performed to study the collision problem between two steel towers with different periods and damping ratios, expose to different values of separation gap and earthquake effects (Chau *et al.* 2003). In the studies by Hong *et al.* (2003), the separation distance between adjacent structures was investigated by considering the structural properties. Three-dimensional collision of two adjacent buildings was investigated under

∗Corresponding author, Associate Professor
E-mail: eaydin@ohu.edu.tr
[a]Associate Professor
E-mail: turankarabork@gmail.com

ISSN: 2092-7614 (Print), 2092-7622 (Online)

earthquake effects with arranged rigid lateral diaphragm for structural behavior with respect to linearity of material (Mouzakis and Papadrakakis 2004). Tubaldi *et al*. (2012) investigated a statistical method for evaluation of the seismic collision risk between neighbor structures. The adjacent concrete structures were examined for different total height and different floor height for collision conditions conditions (Karayannis and Favvata 2005). The demonstrativeness of different impact models was investigated in covering the earthquake collision behavior of neighbor buildings (Muthukumar and DesRoches 2006). The effect of stroke was examined using contact force models for various gaps and validated with nominal impact model without collision phenomena (Raheem 2006). Mahmoud *et al*. (2008) aimed comparison between the nonlinear viscoelastic model and Hertz-damp model considering as Hertz contact rule force-based models in related with non-linear damper. Jankowski (2008) presented a detailed investigation was presented on pounding-involved response of two equal height buildings with substantially different dynamic properties to model the non-linear effects taking place during impact as well as observed in the structural response as the result of earthquake vibrations. A Double Difference Combination (DDC) rule was developed in predicting the separation necessary to prevent seismic pounding between linear structural systems by Garcia and Soong (2009). Soil effects were also examined on the seismic pounding of adjacent building structure under seismic excitations (Shakya and Wijeyewickrema 2009). Khatiwada *et al*. (2014) suggested the Hunt-Crossley model which a general model with a linear or nonlinear force-deformation relationship of building hammerings. Only the earthquake induced structural pounding with all the details identified the models shown and the necessary gaps and necessary recommendations have been given by Jankowski and Mahmoud (2015). A new general spectral difference method (GSDM) was proposed to calculate the minimum safety distances by Yu *et al*. (2017). This pseudo-excitation method was used to derive the relative displacement with respect to random expression of adjacent buildings during earthquakes.

Designing the gap between buildings only will not provide a satisfactory solution in the event of the collapse of anybody and the impact on the other. For this reason, new solutions are needed to improve the dynamic characteristics of the structures and to provide them to behave together. Xu and Zhang (2002), Aldemir and Aydin (2005) also proposed an active control algorithm for adjacent structures. Zhu *et al*. (2001) studied three types control strategies indicating semi-active, active and passive control to avoiding collision. A stochastic optimal coupling-control method for adjacent building structures was presented by Ying *et al*. (2003). Cundumi and Suarez (2008) examined a new control device as a coupling element, which was termed a variable damping semi-active device, consists of two dampers with constant parameters. A structural vibration control strategy has been improved for seismic protection of multi-structure systems that combines inter-structure passive damping elements with local feed-back control systems, which are independently designed and operated, and use semi-active devices with limited actuation capacity as force actuators (Quinonero *et al*. 2012). Quinonero *et al*. (2014) designed a local velocity-feedback energy-peak controller for the seismic protection of a two-building system. An optimal hybrid control approach of two similar adjacent buildings for seismic performance improvement was described for which the passive dampers were used as link members between the two parallel buildings and the active control devices were added as tendon-type devices between two sequential stories in the buildings (Park and Ok 2015).

The effectiveness of MR (Magnetoreological) damper was examined in order to reduce the seismic response of the adjacent multi-storey buildings, including the passive-off, passive and semi-active control strategies by Bharti *et al*. (2010). Uz and Hadi (2014) optimized MR dampers at adjacent structures using integrated fuzzy logic and multi-objective genetic algorithm to avoid the impact damage. Using the fuzzy logic control method by Abdeddaim *et al*. (2016), the acceleration and displacement response of structures were minimized by adding a MR damper placed at the top storey of the building. The optimal design of supplemental dampers allocated uniformly between two adjacent buildings by minimizing the amplitude of a top displacement function of a tall building was estimated to prevent pounding by Luco and De Barros (1998). Xu *et al*. (1999) a parametric study was performed to find optimum damping properties in adjacent buildings with different stiffness ratios and building heights. The results showed that the use of viscous dampers in adjacent buildings of different fundamental frequencies could effectively reduce the earthquake-induced responses of a building. The structure with two different heights was modeled experimentally by connecting with a fluid damper by Yang *et al*. (2003). Zhu and Xu (2005) reported analytical formulas to obtain the most appropriate parameters of the Maxwell model, which describes the fluid dampers used to connect two adjacent structures. Basili and Angelis (2007) studied the optimal passive control of adjacent structures interconnected by nonlinear hysteretic devices. Their study presented that the number of dampers, location and connection type changed the structure behavior positively. Patel and Jangid (2010) deal with the application of viscous damper for response control of seismically excited dynamically similar adjacent coupled structures. Some structural responses such as displacement, accelerations and base shear force were also examined in terms of the reduction of the connected adjacent structures. The main purpose of Bigdeli *et al*. (2012) was to find the optimal placement of a limited number of fluid dampers minimizing interstorey drift. Mazanoglu and Mazanoglu (2017) studied have made the optimization of amount and location of the viscous damper arranged to prevent the collision of the adjacent structures.

The effects of viscoelastic dampers were also investigated for preventing collision of adjacent structures (Zhang and Xu 1999, Patel and Jangid 2014). A complex modal superposition method was used for improving dynamic characteristics of these structures. The inelastic

behavior of adjacent structures connected with viscoelastic dampers from the top was investigated as named building-sky-bridge connections (Kim *et al*. 2006). The design parameters of the connection viscoelastic dampers between two adjacent twin tower structures were optimized by theoretical analyses (Zhu *et al.* 2011). Two optimization criteria were selected in order to minimize the vibration energy of the primary structure and both structures. The results of an experimental study showed that the application of polymer elements placed between the colliding members could mitigate earthquake-induced pounding between adjacent steel structures (Soltysik *et al*. 2017). Abdullah *et al*. (2001) researched the use of shared tuned mass dampers to reduce collision impact on adjacent structures. Shared tuned mass damper's rigidity and damping constants were used as design parameters. An optimally tuned mass damper (TMD) has been proposed for a slender structure surrounded by two more rigid structures than it. A control performance of a pounding tuned mass damper (PTMD) was investigated for reducing the dynamic response of an offshore jacket-type platform structure by (Bekdas and Nigdeli 2012). Some techniques carried out for reducing collision effects of adjacent structures by using shear wall, bracing system and friction dampers (Bhaskararao and Jangid 2006, Hameed *et al*. (2012). In adjacent structures with base isolation systems, the collision is a serious engineering problem. A number of scientific studies have been carried out to solve this problem (Matsagar and Jangid 2005, Komodromos 2008, Polycarpou and Komodromos 2010, Murase *et al*. 2013).

In this study, the optimal designs of the viscous dampers to be placed between adjacent structures having equal height and different dynamic characteristics of structures such as stiffness and mass, which are modeled as shear frames under the effect of earthquake, are investigated to prevent the structural pounding. The relative displacement between the two adjacent structures is defined and included into the proposed algorithm. The drawn relative displacement spectra indicate the risky period ratio under the design earthquake. While minimizing the sum of the damping coefficients of the dampers, it is aimed to reduce the relative displacement defined below the target value. The variations on the period ratio of structures, the upper limit of the damping coefficient of dampers at each storey, the connection type of damper, the vibration mode of structures and the constraint of relative displacement are also investigated in structural models.

2. Generation of the relative displacement spectrum

Spectrum approaches have an important place in building design and are widely used for practical applications in earthquake regulations. A response spectrum is a plot of the peak or steady state response of a series of variable natural period forced to act with the same basic vibration. In the problem of collision of neighbor buildings during earthquake, developing a spectral approach can be important for engineering applications. In the collision problem, relative displacement can reveal risky period ratios for collision under a design earthquake. The period ratio is

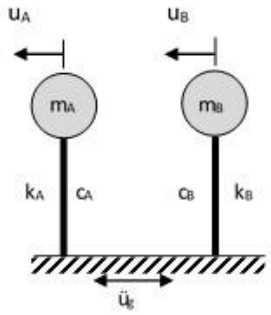

Fig. 1 Mechanical reduced model of adjacent structures

defined as the rate of periods of adjacent structures to each other. In adjacent structures, relative displacement spectra can be created for design earthquakes and the band of the most dangerous period ratios can be observed. This will be an important as a design tool for engineers to prevent collision.

The mechanical model of adjacent structures can be shown in Fig. 1 to each with a single degree of freedom. In the left and right structure is shown as named *A* and *B* in Fig. 1. Here, k_A, k_B, c_A, c_B, m_A and m_B denote the stiffness coefficients, structural damping coefficients and masses of *A* and *B* structures, respectively. The uncoupled equations of the models exposed to ground motion are written as follows

$$m_A\ddot{u}_A + c_A\dot{u}_A + k_A u_A = -m_A\ddot{u}_g \quad (1)$$

$$m_B\ddot{u}_B + c_B\dot{u}_B + k_B u_B = -m_B\ddot{u}_g \quad (2)$$

Where u_A, $\dot{u}_A$, $\ddot{u}_A$ denote the displacement, the velocity and the acceleration of the structure *A*. This definition is similar for the structure *B*. The parameter $\ddot{u}_g$ is the horizontal acceleration of the ground motion. Eqs. (1)-(2) in the matrix-vector form can be rewritten again as follows

$$\begin{bmatrix} m_A & 0 \\ 0 & m_B \end{bmatrix}\begin{Bmatrix} \ddot{u}_A \\ \ddot{u}_B \end{Bmatrix} + \begin{bmatrix} c_A & 0 \\ 0 & c_B \end{bmatrix}\begin{Bmatrix} \dot{u}_A \\ \dot{u}_B \end{Bmatrix} + \begin{bmatrix} k_A & 0 \\ 0 & k_B \end{bmatrix}\begin{Bmatrix} u_A \\ u_B \end{Bmatrix} = -\begin{bmatrix} m_A & 0 \\ 0 & m_B \end{bmatrix}\begin{Bmatrix} 1 \\ 1 \end{Bmatrix}\ddot{u}_g \quad (3)$$

Relative displacement between adjacent buildings can be expressed as the difference between the displacements of structures A and B as follows (Ying *et al*. 2003)

$$RD = u_B - u_A \quad (4)$$

The behavior of adjacent structures exposed to ground motion usually occurs in four different types as seen in Fig. 2. Structures display either phase-out or phase-in behavior during an earthquake. If the vibration characteristics of adjacent structures are similar, a structural response as seen in Figs. 2(a)-(b) occurs at any time t. Because the dynamic responses of the structures are compatible with each other, the risk of pounding will decrease. However, if the structures have different dynamic characteristics, the vibrations of the structures will be out of phase. They will either move away from each other or close to each other at any time of the earthquake, as in Figs. 2(c)-(d). As shown in Fig 2(d), the relative displacement expressed by the Eq. (4), which is positive, increases the risk of collision. Therefore, in order to prevent collision between structures, the relative

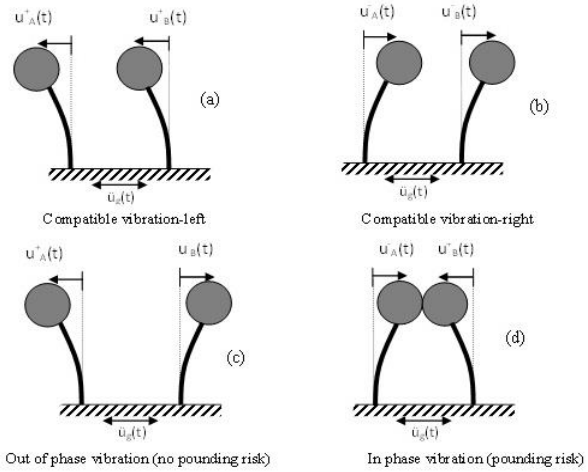

Fig. 2 Vibration behavior scenarios of adjacent structures (a) Compatible vibration-left (b) Compatible vibration-right (c) Out of phase vibration (no pounding risk) (d) In phase vibration (pounding risk)

displacement given in Eq. (4) can be defined as a control parameter. If the relative displacement (RD) defined in Eq. (4) is inserted into the Eq. (3) and rewritten as

$$\begin{bmatrix} m_A & 0 \\ m_B & m_B \end{bmatrix} \begin{Bmatrix} \ddot{u}_A \\ \ddot{RD} \end{Bmatrix} + \begin{bmatrix} c_A & 0 \\ c_B & c_B \end{bmatrix} \begin{Bmatrix} \dot{u}_A \\ \dot{RD} \end{Bmatrix} + \begin{bmatrix} k_A & 0 \\ k_B & k_B \end{bmatrix} \begin{Bmatrix} u_A \\ RD \end{Bmatrix} = -\begin{bmatrix} m_A & 0 \\ 0 & m_B \end{bmatrix} \begin{Bmatrix} 1 \\ 1 \end{Bmatrix} \ddot{u}_g \quad (5)$$

The structural vibration parameters of the primary structure (A) can be kept constant and the stiffness of the secondary structure (B) can be changed with small increments. The changes in the relative displacement can be calculated as a result of the analysis made in the time domain in each change. The maximum values of the relative displacement in the positive region can be selected. For any damping ratio, as a result of the time history analyses under the selected design earthquake, the maximum relative displacements with respect to the period ratio of neighbor buildings can be plotted as a response spectrum. These spectrum graphs drawn under the selected design earthquake will give information about the period at which the collision risk will occur. Using the proposed relative displacement spectra, the gap between the structures can be appropriately adjusted, and the structure to be built next to an existing structure can be designed to prevent collision.

2.1 Relative displacement spectra for El Centro (NS) earthquake record

A sample design earthquake is used in order to determine the period ratios with a high risk of collision. In this section, a sample study is performed for the relative displacement spectrum graphs mentioned in the previous section using El Centro earthquake acceleration record (NS). The findings will be used in the numerical sample section of this study during the implementation of the proposed damper optimization method. The mechanical model of the single degree of freedom adjacent structures discussed in the study is shown in Fig. 1. The structural characteristics of the

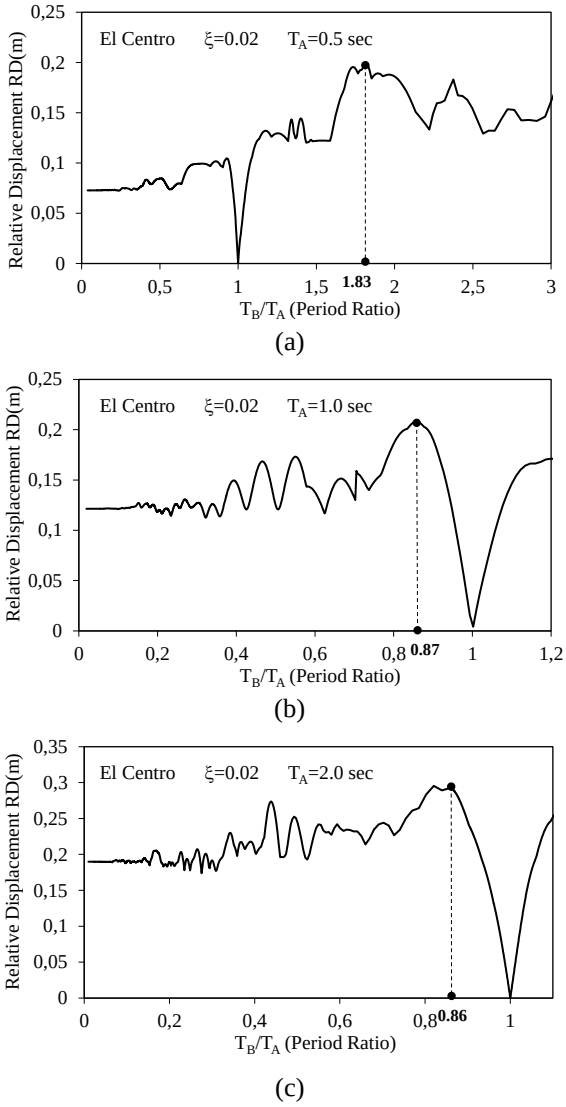

Fig. 3 Relative displacement spectrums (a) T_A=0.5 sec (b) T_A=1.0 sec (c) T_A=2.0 sec

selected building models are shown in Table 1. The vibration period of the structure (A) is assumed to be constant and the stiffness of the other structure is changed over a wide band to increase the vibration period of the structure (B) in small amounts. In each increment, the period ratios of the two structures are changed and time history analyses are performed by using El Centro earthquake acceleration record (NS). The maximum (positive sign) values of relative displacement between the structures are calculated and are plotted according to the variation of period ratio.

Firstly, the period of the primary structure (A) and structural damping ratio of structures were chosen as 0.5 sec and 0.02 respectively. It is analyzed by changing the stiffness of structure (B) and the relative displacement of the structures with respect to period ratios is shown in Fig. 3(a). When the period of the first structure is 0.5 s, the maximum relative displacement between adjacent structures is peaked at a critical period ratio (T_B/T_A=1.83). In the case where the period ratio of the adjacent structures is equal to 1, the maximum relative displacement approaches zero, in which

Table 1 The variation of structural properties

Period T_A (sec)	0.5	1.0	2.0
Mass m_A (kg)	75000	75000	75000
Mass m_B (kg)	75000	75000	75000
Stiffness k_A (N/m)	11843525	2960881	740220.33
Stiffness k_B (N/m)	1120-8000000000	1120-8000000000	1120-8000000000
Damping Ratio ζ	0.02	0.02	0.02

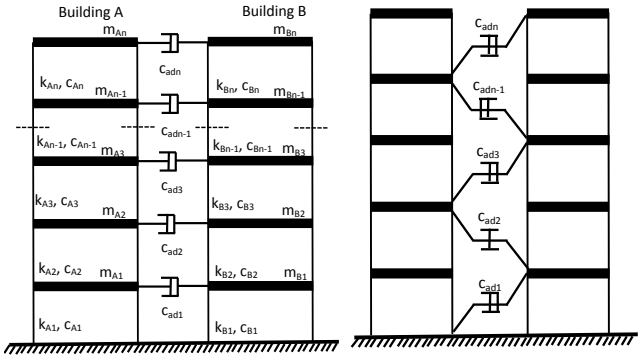

Fig. 4 Adjacent model structures

case the structures vibrate in the same phase and there is no risk of pounding between structures. In the case where T_A is equal to 1.0 sec and 2 sec, the approximate period ratios where the collision risks of adjacent structures can occur at some critical period ratios (T_B/T_A=0.87, 0.86) as shown in Figs. 3(b)-(c). A specific structural damping ratio, a certain period ratio band and the change in design earthquake can be investigated. Research can be expanded for different structural damping ratios and different design earthquakes. Furthermore, the period ratios of adjacent structures can be examined at greater intervals. In this case, larger relative displacement (RD) peaks create more collision risk. However, the increase of period ratios means that one of the adjacent structures has an extremely long or short period. In practice, the probability of encountering this situation is very rare.

3. Formulation of the problem for adjacent buildings

Two adjacent n-storey buildings at the same level and the viscous damper designs to be placed between buildings to prevent collision are shown in Fig. 4. In the design showed in Fig. 4(a) and named to as the classical-model, the dampers connect two buildings at floor levels. In the design which is called as the stair-model, the dampers placed on each floor connect two sequential storeys (Fig. 4(b)). The damper design is called *X*-diagonal model, which is placed between the structures in Fig. 4(c). In the without damper case, the equations of motion of the structures *A* and *B* can be written in the uncoupled form as follows

$$\boldsymbol{M_A\ddot{U}_A(t) + C_A\dot{U}_A(t) + K_AU_A(t) = -M_Ar\ddot{U}_g(t)} \quad (6)$$

$$\boldsymbol{M_B\ddot{U}_B(t) + C_B\dot{U}_B(t) + K_BU_B(t) = -M_Br\ddot{U}_g(t)} \quad (7)$$

While $\boldsymbol{U_A(t)}$ and $\boldsymbol{U_B(t)}$ denote the displacement vectors, $\boldsymbol{\dot{U}_A(t)}$ and $\boldsymbol{\dot{U}_B(t)}$ are the velocity of A and B buildings in vector form. The parameters of $\boldsymbol{\ddot{U}_A(t)}$ and $\boldsymbol{\ddot{U}_B(t)}$ mean the vector of acceleration for A and B buildings and the ground acceleration is defined as $\ddot{U}_g$. The mass matrices are expressed with $\boldsymbol{M_A}$ and $\boldsymbol{M_B}$, $\boldsymbol{C_A}$ and $\boldsymbol{C_B}$ are structural damping matrices, the stiffness matrices for A and B buildings are $\boldsymbol{K_A}$ and $\boldsymbol{K_B}$. The parameter $\boldsymbol{r}$ is influence coefficient vector for a base input. In without damper case, the governing equation of building models can be given in coupled form as follows

$$\boldsymbol{M\ddot{U}(t) + C\dot{U}(t) + KU(t) = -Mr\ddot{U}_g(t)} \quad (8)$$

Here, the structural mass, damping, and stiffness matrices of coupled system are written as

$$\boldsymbol{M = \begin{bmatrix} M_A & 0 \\ 0 & M_B \end{bmatrix}_{2nx2n} \quad K = \begin{bmatrix} K_A & 0 \\ 0 & K_B \end{bmatrix}_{2nx2n}}$$
$$\boldsymbol{C = \begin{bmatrix} C_A & 0 \\ 0 & C_B \end{bmatrix}_{2nx2n}} \quad (9)$$

$\boldsymbol{C}$ denotes the structural damping matrix which can be calculated proportionately with mass and stiffness. When dampers are added between structures, the equation of motion can be rewritten as follows

$$\boldsymbol{M\ddot{U}(t) + (C + C_{ad})\dot{U}(t) + KU(t) = -Mr\ddot{U}_g(t)} \quad (10)$$

where $\boldsymbol{C_{ad}}$ includes the damping coefficients of the manufactured viscous dampers. Since these viscous absorbers have different connection points in each type of design as shown in Fig. 4, $\boldsymbol{C_{ad}}$ will change in each model type. $\boldsymbol{C_{ad}}$ is an added damping matrix that should be calculated by minimizing an objective function. $\boldsymbol{C_{ad}}$ in classical-model, stair-model and X-diagonal model can be given as follows

$$C_{ad} = \begin{array}{c} \begin{matrix} 1 & 2 & 3 & \cdots & n & n+1 \end{matrix} \\ \begin{bmatrix} c_{ad1} & 0 & 0 & \cdots & 0 & -c_{ad1} \\ 0 & c_{ad2} & 0 & \cdots & 0 & 0 \\ 0 & 0 & c_{ad3} & \cdots & 0 & 0 \\ \vdots & \vdots & \vdots & \vdots & \vdots & \vdots \\ 0 & 0 & 0 & \cdots & c_{adn} & 0 \\ -c_{ad1} & 0 & 0 & \cdots & 0 & c_{ad1} \\ 0 & -c_{ad2} & 0 & \cdots & 0 & 0 \\ \vdots & \vdots & \vdots & \vdots & \vdots & \vdots \\ 0 & 0 & 0 & \cdots & 0 & 0 \\ 0 & 0 & 0 & \cdots & 0 & 0 \\ 0 & 0 & 0 & \cdots & -c_{adn} & 0 \end{bmatrix} \end{array}$$

$$
\begin{array}{cccccc}
n+2 & & 2n-2 & 2n-1 & 2n & \\
0 & \cdots & 0 & 0 & 0 & 1 \\
-c_{ad2} & \cdots & 0 & 0 & 0 & 2 \\
0 & \cdots & 0 & 0 & 0 & 3 \\
\vdots & \vdots & \vdots & \vdots & \vdots & \cdots \\
0 & \cdots & 0 & 0 & -c_{adn} & n \\
0 & \cdots & 0 & 0 & 0 & n+1 \\
c_{ad2} & \cdots & 0 & 0 & 0 & n+2 \\
\vdots & \vdots & \vdots & \vdots & \vdots & \cdots \\
0 & \cdots & c_{adn-2} & 0 & 0 & 2n-2 \\
0 & \cdots & 0 & c_{adn-1} & 0 & 2n-1 \\
0 & \cdots & 0 & 0 & c_{adn} & 2n
\end{array}
$$

$$
C_{ad} = \begin{bmatrix}
0 & 0 & 0 & \cdots & 0 \\
c_{ad2} & 0 & 0 & \cdots & 0 \\
0 & c_{ad3} & 0 & \cdots & 0 \\
\vdots & \vdots & \vdots & \vdots & \vdots \\
0 & 0 & 0 & \cdots & 0 \\
0 & 0 & 0 & \cdots & 0 \\
-c_{ad2} & 0 & 0 & \cdots & 0 \\
\vdots & \vdots & \vdots & \vdots & \vdots \\
0 & 0 & 0 & \cdots & 0 \\
0 & 0 & 0 & \cdots & 0 \\
0 & 0 & 0 & \cdots & 0
\end{bmatrix}
$$

$$
\begin{bmatrix}
-c_{ad1} & 0 & \cdots & 0 & 0 & 0 \\
0 & -c_{ad2} & \cdots & 0 & 0 & 0 \\
0 & 0 & \cdots & 0 & 0 & 0 \\
\vdots & \vdots & \vdots & \vdots & \vdots & \vdots \\
0 & 0 & \cdots & 0 & 0 & -c_{adn} \\
c_{ad1} & 0 & \cdots & 0 & 0 & 0 \\
0 & c_{ad2} & \cdots & 0 & 0 & 0 \\
\vdots & \vdots & \vdots & \vdots & \vdots & \vdots \\
0 & 0 & \cdots & c_{adn-2} & 0 & 0 \\
0 & 0 & \cdots & 0 & c_{adn-1} & 0 \\
0 & 0 & \cdots & 0 & 0 & c_{adn}
\end{bmatrix}
$$

$$
C_{ad} = \begin{bmatrix}
c_{ad1}+c_{ad2} & 0 & 0 & \cdots & 0 \\
0 & c_{ad2}+c_{ad3} & 0 & \cdots & 0 \\
0 & 0 & c_{ad3}+c_{ad4} & \cdots & 0 \\
\vdots & \vdots & \vdots & \vdots & \vdots \\
0 & 0 & 0 & \cdots & c_{ad12} \\
0 & -c_{ad2} & 0 & \cdots & 0 \\
-c_{ad2} & 0 & -c_{ad3} & \cdots & 0 \\
\vdots & \vdots & \vdots & \vdots & \vdots \\
0 & 0 & 0 & \cdots & 0 \\
0 & 0 & 0 & \cdots & -c_{ad2} \\
0 & 0 & 0 & \cdots & 0
\end{bmatrix}
$$

$$
\begin{bmatrix}
0 & -c_{ad2} & \cdots & 0 & 0 & 0 \\
-c_{ad2} & -c_{ad2} & \cdots & 0 & 0 & 0 \\
0 & -c_{ad3} & \cdots & 0 & 0 & 0 \\
\vdots & \vdots & \vdots & \vdots & \vdots & \vdots \\
0 & 0 & \cdots & 0 & -c_{ad2} & 0 \\
c_{ad1}+c_{ad2} & 0 & \cdots & 0 & 0 & 0 \\
0 & c_{ad2}+c_{ad3} & \cdots & 0 & 0 & 0 \\
\vdots & \vdots & \vdots & \vdots & \vdots & \vdots \\
0 & 0 & \cdots & c_{adn-2}+c_{adn-1} & 0 & 0 \\
0 & 0 & \cdots & 0 & c_{adn-1}+c_{adn} & 0 \\
0 & 0 & \cdots & 0 & 0 & c_{ad1n}
\end{bmatrix}
\quad (11)
$$

It can be decomposed into corresponding to the damping coefficients of added dampers and is written as

$$\boldsymbol{C_{ad}} = c_{ad1}\frac{\partial \boldsymbol{C_{ad}}}{\partial c_{ad1}} + c_{ad2}\frac{\partial \boldsymbol{C_{ad}}}{\partial c_{ad2}} + \ldots + c_{adn}\frac{\partial \boldsymbol{C_{ad}}}{\partial c_{adn}} \quad (12)$$

where $c_{adi}\,(i = 1,2,\ldots,n)$ corresponds to the damping coefficient of the ith added damper and the partial derivative of $\boldsymbol{C_{ad}}$ ($\frac{\partial \boldsymbol{C_{ad}}}{\partial c_{adi}}$) denotes the location matrix of the ith added damper. Considering ith mode, the equation can be written as

$$2\zeta_i\,\omega_i = \frac{\boldsymbol{\phi_i^T}(\boldsymbol{C}+\boldsymbol{C_{ad}})\boldsymbol{\phi_i}}{\boldsymbol{\phi_i^T M \phi_i}} = \frac{\boldsymbol{\phi_i^T C \phi_i}}{\boldsymbol{\phi_i^T M \phi_i}} + \frac{\boldsymbol{\phi_i^T C_{ad}\,\phi_i}}{\boldsymbol{\phi_i^T M \phi_i}} \quad (13)$$

After dampers are added to the structure, the damping ratio of the system is defined as ζ_i . The normalized vector of i^{th} mode is represented as $\boldsymbol{\phi_i}$, and ω_i indicates the undamped natural circular frequency of ith mode of the structural system. The proportional damping matrix is included in the Eq. (13). There exists no coupling between any other modes and i^{th} mode. This case is represented as

$$\frac{\boldsymbol{\phi_i^T C \phi_j}}{\boldsymbol{\phi_i^T M \phi_j}} = \begin{cases} 2\zeta_{sti}\,\omega_i & i = j \\ 0 & i \neq j \end{cases} \quad (14)$$

The structural damping ratio is symbolized as ζ_{sti} for ith mode. It can be conveniently presumed to simplify the formulation of the problem as follows

$$\frac{\boldsymbol{\phi_i^T C_{ad}\,\phi_j}}{\boldsymbol{\phi_i^T M \phi_j}} = \begin{cases} 2\zeta_{adi}\omega_i & i = j \\ 0 & i \neq j \end{cases} \quad (15)$$

The added damping ratio of ith mode is prescribed as ζ_{adi}. Eq. (13) are rewritten using Eqs. (14)-(15) as follows

$$\zeta_i = \zeta_{sti} + \zeta_{adi} \quad (16)$$

ζ_{sti} is generally known according to the types of structures such as in reinforced structures (0.05) and steel structures (0.02). ζ_i is the target damping ratio and ζ_{adi} denotes the added damping ratio. If ζ_{sti} and ζ_i are given, the added damping ratio can be calculated as

$$2\zeta_{adi}\,\omega_i = \frac{\boldsymbol{\phi_i^T C_{ad}\,\phi_i}}{\boldsymbol{\phi_i^T M \phi_i}} = c_{ad1}\frac{\boldsymbol{\phi_i^T}\frac{\partial \boldsymbol{C_{ad}}}{\partial c_{ad1}}\boldsymbol{\phi_i}}{\boldsymbol{\phi_i^T M \phi_i}} + c_{ad2}\frac{\boldsymbol{\phi_i^T}\frac{\partial \boldsymbol{C_{ad}}}{\partial c_{ad2}}\boldsymbol{\phi_i}}{\boldsymbol{\phi_i^T M \phi_i}} + \cdots + c_{adn}\frac{\boldsymbol{\phi_i^T}\frac{\partial \boldsymbol{C_{ad}}}{\partial c_{adn}}\boldsymbol{\phi_i}}{\boldsymbol{\phi_i^T M \phi_i}} \quad (17)$$

where a new parameter λ_s can be defined as

$$\lambda_s = \frac{\boldsymbol{\phi_i^T}\frac{\partial \boldsymbol{C_{ad}}}{\partial c_{ads}}\boldsymbol{\phi_i}}{\boldsymbol{\phi_i^T M \phi_i}} \qquad (s=1, 2, .., n) \quad (18)$$

To derive the added damping ratio, Eq. (17) can be rewritten by arranging as follows

$$\zeta_{adi} = \frac{1}{2\omega_i}(\lambda_1 c_{ad1} + \lambda_2 c_{ad2} + \cdots + \lambda_n c_{adn}) = \frac{1}{2\omega_i}\sum_{s=1}^{n}\lambda_s c_{ads} \quad (19)$$

4. Damper optimization problem in adjacent structures

Many different objective functions, such as the structural

top displacement, the absolute acceleration, the base shear force and moment, the sum of interstorey drifts, the maximum interstorey drift, some of energy parameters and cost minimization, are used alone or in combination in damper optimization problems. While defining the optimization problem, some constraints are suggested considering both structural behavior and practical applications. In the case of structural optimization problems, cost is an important phenomenon. These technological elements, which have been used for the control of the structures in recent years, increase the cost of the building significantly. Since the increase in the capacity of the dampers will lead to an increase in the damping coefficients, the need to minimize the sum of the damping coefficients comes from an economic perspective. The sum of the damping coefficients of dampers is chosen as proposed objective function to be minimized; it can be given as

$$\text{Min. } f = \sum_{i=1}^{n} c_{adi} \tag{20}$$

An equality constraint can be considered in terms of added damping ratio as below

$$\zeta_{adi} = \frac{1}{2\omega_i}(\lambda_1 c_{ad1} + \lambda_2 c_{ad2} + \cdots + \lambda_n c_{adn}) \tag{21}$$

ω_i and λ_s can be calculated using Eigen analysis. All optimization functions linearly depend on the design parameters. The upper and lower limits of the design variables, the inequality constraints are given as

$$0 \le c_{adi} \le \bar{c}_i \qquad (\text{i} = 1,2,\ldots,\text{n}) \tag{22}$$

The parameter $\bar{c}_i$ is defined as the upper limit of the i^{th} design variables. The variation of $\bar{c}_i$ can affect the optimal design of damper.

4.1 Solution algorithm

Some optimization methods have been improved such as gradient based algorithms (Takewaki 1997, Takewaki 2000, Aydin *et al*. 2007), swarm algorithms such as artificial bee and ant colony algorithms (Amini and Ghaderi 2013, Sonmez *et al*. 2013), genetic algorithms and fuzzy logic algorithms (Uz and Hadi 2014) in damper optimization. A novel algorithm has been developed for the optimum design of viscous dampers placed between adjacent structures under the earthquake effect, including the objective function and constraints mentioned in the previous section. Since the aim and the constraints functions are linear functions of design variables, the problem is easy to solve. To find the optimal values of damping coefficients under constraints by minimizing the objective function, some of optimization algorithms such as Differential Evolution, Nelder Mead and Simulated Annealing are used (Wolfram Research 2003). These three numerical minimization methods have been applied to create an algorithm of optimal damper design (Aydin 2013).

The process steps of the algorithm given in Fig. 5 can be summarized as follows:

Step 1. Compose the relative displacement spectra using a design earthquake record (El Centro- NS) as mentioned in section 2.1.

Step 2. Read the the structural stiffness matrix (K), and mass matrix (M), Select the upper limit of the design variable $\bar{c}_i$ and the allowable level of relative displacement $\overline{RD}$. Determine the critical period ratio (T_B/T_A) versus the maximum relative displacement over a certain period band using the drawn spectra for the earthquake.

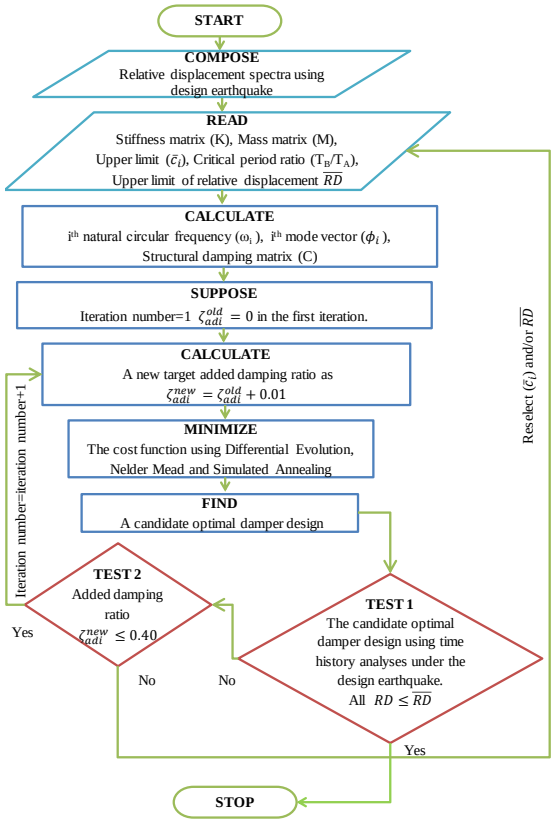

Fig. 5 Flowchart of proposed algorithm

Step 3. Calculate ω_i, ϕ_i, C for i^{th} mode.

Step 4. Take iteration number=1 at the beginning of the algorithm.

Step 5. Calculate $\zeta_{adi}^{new} = \zeta_{adi}^{old} + 0.01$ while assume $\zeta_{adi}^{old} = 0$ in the first iteration. ζ_{adi}^{new} is raised by 1% at each iteration.

Step 6. Minimize the objective function given in Eq. (20) according to constraints of Eqs. (21)-(22). Adopt the numerical minimization module of Mathematica 5.0 (Wolfram Research 2003) to solve the linear optimization problem by conducting three different methods, i.e., Differential Evolution, Nelder Mead, and Simulated Annealing.

Step 7. Find an optimal damper design as a candidate.

Step 8. Test the candidate design calculated in Step 7 using linear time history analysis. In this test, compute $RD_i = \{U_{Bi}(t) - U_{Ai}(t)\}^{peak}$ for i=1,…n. If all RD computed are below the desired level ($RD \le \overline{RD}$), then finished the algorithm. Otherwise, return test 2 as shown in flowchart.

Step 9. Control the added damping ratio as $\zeta_{adi}^{new} \le 0.40$. The maximum damping ratio which can be reached by adding dampers in building type structures is chosen as 0.40. If this step is satisfied, go to step 5 and repeat the

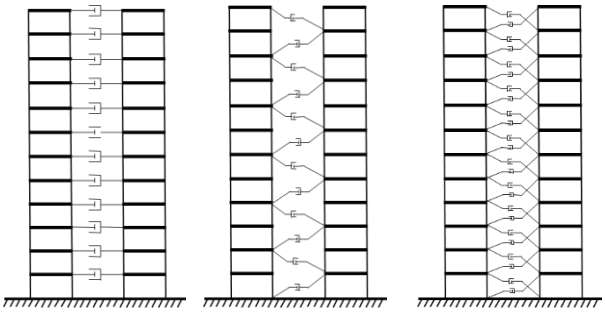

(a) Classical Model (b) Stair Model (c) X-diagonal Model

Fig. 6 12-Storey adjacent structures and damper placement models

iteration by increasing the target damping rate. If this condition is not satisfied, go to step 2 and reselect $\bar{c}_i$ and/or $\overline{RD}$ again.

To solve optimization problems, Differential Evolution, Nelder Mead and Simulated Annealing are commonly used. Differential Evolution is a direct optimization method that is a fast and quite robust stochastic parallel search evolution strategy. Differential Evolution method is a preferred method of solving no differentiable, non-linear and multimodal objective functions. The Nelder-Mead method, a direct search procedure, for a function of variables, the algorithm maintains a set of points that form the corners of a polytope n-dimensional space. Simulated Annealing is also a simple stochastic function minimization which results from the physical annealing process in which a metal object is heated to a high temperature and allowed to cool slowly. The process allows the atomic structure of the metal to settle in a lower energy state and thus become a harder metal (Wolfram Research 2003). These methods display the good consistency between them.

El Centro (NS) earthquake record is only used in this study. Different earthquake records or generated earthquake records can be used as a design earthquake. The determination of $\bar{c}_i$ may vary according to production standards and application practices. $\overline{RD}$ can also be considered as the sum of the peak displacements between the two neighbor structures given by the designer or given in the regulations. The different selections of these parameters are examined.

5. Numerical example

Fig. 6 shows 12-storey adjacent structures and the dampers placed between them for three different damper designs. The design in which the dampers are placed in parallel between the adjacent structures at the floor levels is called the classical model (Fig. 6(a)). Fig. 6(b) shows the stair model, which dampers are connected to sequential storeys of buildings A and B. Adjacent structures are linked with dampers placed diagonally and the X-diagonal model is formed in Fig. 6(c). In this section of the study, the effects of total damping capacity $\bar{c}_i$ at each storey, allowable levels of relative displacement, critical period ratio T_B/T_A, and different response modes on the optimum placement of dampers for each model are investigated.

Table 2 Structural properties of buildings *A* and *B*

m_A (kg)×10^4	10.0	20.0	31.99
m_B (kg)×10^4	6.4	6.156	23.007
k_A (N/m)×10^7	100	50.0	20.0
k_B (N/m)×10^7	16.83	19.0	19.0
T_A (sec)	0.5	1.0	2.0
T_B (sec)	0.915	0.87	1.72
T_B/T_A	1.83	0.87	0.86

Table 3 Parameter limits and damper design types for model cases

Damper design type*	Classical (CL), Stair (ST), X-diagonal (X)
Corresponding mode	1-2
Period ratio T_B/T_A	1.83-0.87-0.86
Upper limit of damping coefficient $\bar{c}_i$ (Nsec/m)×10^6	1-2
Allowable level of relative displacement $\overline{RD}$ (cm)	5-8-10

*Case: Damper design type-Mode number-Period ratio-Damping coefficient-Relative displacement

The storey stiffness and mass, the critical period ratios of the structures *A* and *B*, the corresponding period values, are given in Table 2. These critical period ratios are set to equal the peak values for El Centro earthquake record shown in Fig. 3, and the most risky conditions for pounding are taken into account. The damper design type, the corresponding mode, the period ratio, the upper limit of damping coefficient and the allowable level of relative displacement are given in Table 3. The design models are coded according to the symbol and numerical values shown in Table 3. For example; CL-2-1.83-2-8: in the case of the classical damper design, taking into account the 2nd mode behavior, the period ratio of 1.83, limit damping coefficient of 2×10^6 Nsec/m and the allowable relative displacement of 8 cm are coded.

The maximum relative displacement between the adjacent structures indicates the minimum space to be designed between buildings. During the design and construction of adjacent buildings, this gap must be determined according to the conditions of the earthquake regulations. The explanations in the Turkish Building Earthquake Code (2019) are given as follows: "The minimum amount of gap to be released shall be at least 30 mm up to 6 m height and at least 10 mm for every 3 m height after 6 m". In this study, the allowable level of relative displacement can be taken as a minimum gap as 5 cm, 8 cm and 10 cm, respectively. According to the Turkish Building Earthquake Code (2019), a minimum gap of 13 cm is required for 12 storey buildings which have each storey height of 3m. The probability of collision of the structures is simulated by selecting the allowable level smaller than 13 cm. In fact, the gap levels given in the earthquake regulations apply to situations where the structures do not contain any dampers, in the case of the additional dampers between the adjacent structures; this gap must be reconsidered in the earthquake design codes.

As a result of the analysis of the models, it is observed

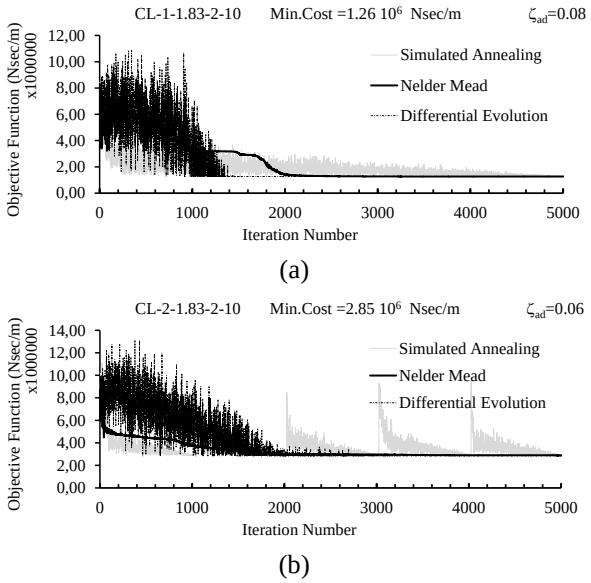

Fig. 7 The variation of the objective function according to the iteration number in numerical optimization for three numerical optimization methods in case of (a) Mode 1 and (b) Mode 2 in classical model

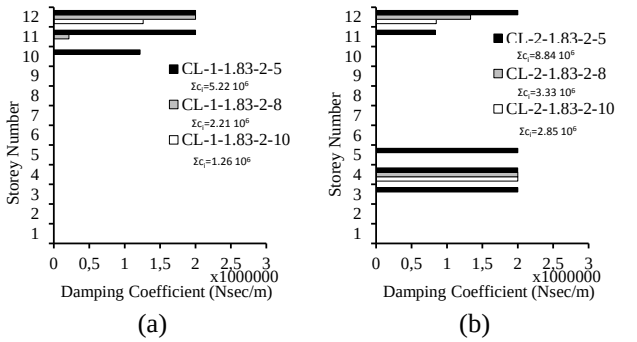

Fig. 8 Optimum distribution of damping coefficients for the change of $\overline{RD}$ in case of (a) Mode 1and (b) Mode 2 in classical mode

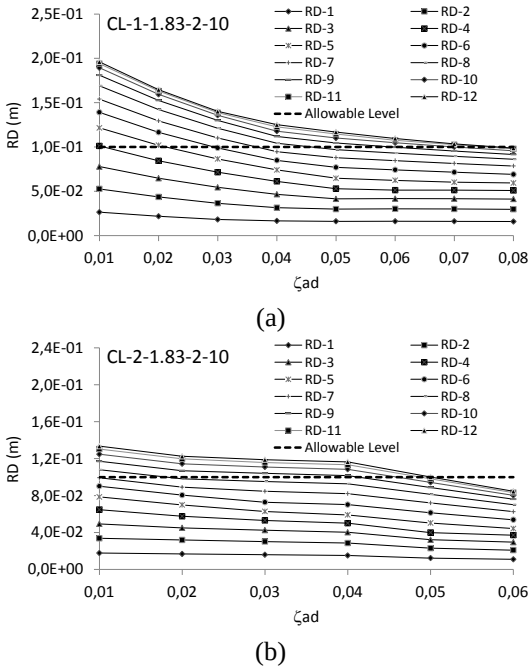

Fig. 9 The variation of relative displacements according to added damping ratio in case of (a) Mode 1 and (b) Mode 2 in classical model

that some models do not require a damper because there is no risk of collision. This means that the calculated relative displacement *RD* does not reach the allowable level $\overline{RD}$. In some models, the relative displacements (*RD*) on some storeys cannot be lowered below the target relative displacements ($\overline{RD}$), since the upper limit for each added damper is not sufficient. The limit value of added damping ratio in this study is 40%, which is acceptable for building type structures. In these models some relative displacements cannot be reduced to the desired level even though this limit value is reached. In other models, the optimum damper distributions are found to be successful.

5.1 Classical model

The dampers are connected in parallel with the storey levels of the two adjacent buildings in the classical model as shown in Fig. 6(a). The changes of the objective functions for three numerical optimization methods at last step are plotted as the structural response corresponds to the first and second mode in Fig 7. Differential Evolution, Nelder Mead and Simulated Annealing, are employed by comparing the results. Considering both the first and the second mode, it can be seen from the variation of objective function during the numerical optimization in the last step that three different methods converge to the same minimum value.

The effects of the limit value of damping coefficient in each storey $\bar{c}_i$, the allowable limit of relative displacement $\overline{RD}$, period ratio T_B/T_A and the effect of mode behavior on the damper distribution are investigated. For this purpose, the effect of the changes of the mentioned parameters is examined by choosing between the models which are positive. In the case of the first mode in Fig. 8(a) and the second mode in Fig. 8(b), selecting $\bar{c}_i = 2 \times 10^6$ Nsec/m, the period ratio is taken as 1.83 and the optimal damper distribution is found for 5 cm, 8 cm and 10 cm of $\overline{RD}$. In Fig. 8(a), when the first mode is considered, it is shown that the critical region of the collision is the upper storeys. When $\overline{RD}$ has large values, it is seen that the damper distribution is concentrated on the upper storeys, and in case of $\overline{RD}$ decrease, it is determined that dampers are also needed from the top storey down to the lower storey. The increase in the limit relative displacement leads to a decrease in the amount of damper used. Therefore, the cost of the damper is also reduced. When the second mode behavior is taken into account, it is seen that the top and middle storeys are the critical regions for pounding (Fig. 8(b)). In these critical zones, more dampers are needed as $\overline{RD}$ decreases. If the effect of the mode behavior is compared, in the second mode, the dampers are distributed over more storeys and more dampers are needed in Figs. 8(a)-(b).

When the models CL-1-1.83-2-10 and CL-2-1.83-2-10 are selected in Fig. 8, it is seen in Fig. 9 that the relative

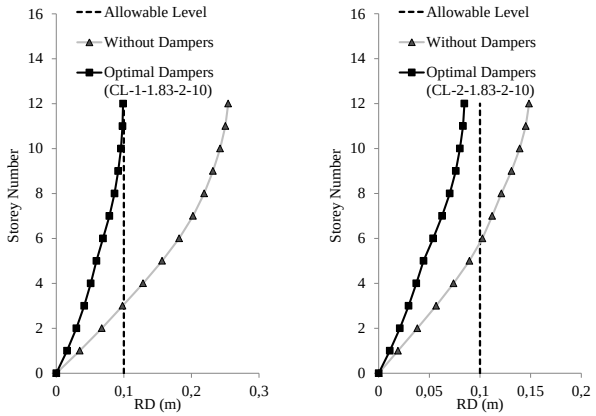

(a) (b)

Fig. 10 Peak relative displacement values for optimal damper design in case of (a) Mode 1 and (b) Mode 2 in classical model

displacements on all floors are reduced below the allowable relative displacement for first and second modes. The added damping ratio takes as the value of 8% in the end of the algorithm for the first mode control as presented in Fig. 9(a), while the result of the damper distribution is reached in the case of a damping ratio of 6% for the second mode (Fig. 9(b)). Fig. 10 shows that the peak relative displacements at storey levels for these models are reduced below the target levels to reduce the risk of collisions. Furthermore, the values of RD exceeding the allowable limit in the without damper case are reduced below this limit by optimal addition of dampers.

When the first and second mode behaviors are taken into account, the effect of the change of the limit of the damping coefficient ($\bar{c}_i$) on the optimum damper distribution is investigated in Fig. 11. In both modes, the reduction in the amount of damper limits causes the damper distribution to be placed on more storey. In the damper design according to the first mode, the dampers are placed on the upper floors where the risk of collision is high (Fig. 11(a)). In the second mode, the risk of collision is on both the upper and the middle floors, so that the damper settlements focus on these floors (Fig. 11(b)). When $\bar{c}_i$ increases in case of the first mode, the total amount of damper increase. However, taking into account the second mode, the increase in $\bar{c}_i$ decreases the total amount of optimal damper. This demonstrates that the variation of the mode considered changes the optimum damper distribution and the total damper quantity.

The period of structure A is chosen as three different values as T_A=0.5 sec; 1.0 sec; 2.0 sec and the critical period ratios corresponding to them are calculated as T_B/T_A=1.83; 0.87; 0.86 as shown in Fig. 3. In the case of T_A=1.0 sec; 2.0 sec, the critical period ratios are close to each other as 0.87 and 0.86. Damper designs corresponding to these period ratios are very close to each other, as seen in the first mode (Fig. 12(a)). In case T_A=0.5 sec, this is the risky pounding situation where the period ratio is highest, according to Fig. 12(a) where the total amount of damper is the lowest compared to the others. When the second mode is taken into consideration, it is seen in Fig. 12(b) that the maximum damper quantity is obtained for the model with T_A=1.0 sec.

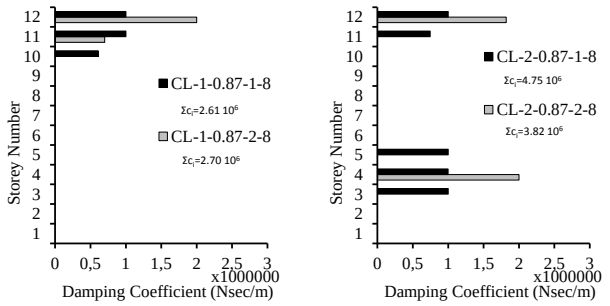

(a) (b)

Fig. 11 Optimum distribution of damping coefficients for the change of $\bar{c}_i$ in case of (a) Mode 1and (b) Mode 2 in classical model

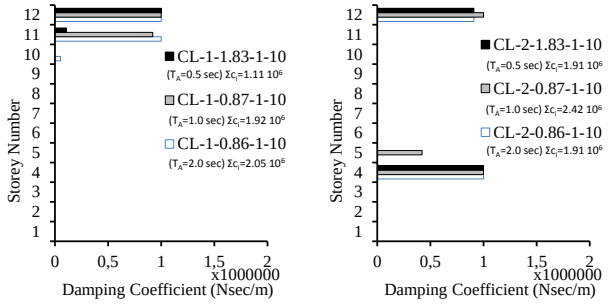

(a) (b)

Fig. 12 Optimum distribution of damping coefficients for the change of T_B/T_A in case of (a) Mode 1and (b) Mode 2 in classical model

5.2 Stair model

To avoid from pounding, the dampers are connected to sequential storeys of adjacent buildings in the stair model as shown in Fig. 6(b). Similar to the classical model analysis, the effects of $\overline{RD}$, $\bar{c}_i$, T_B/T_A and the mode effect on optimum damper distribution are examined here. The stair damper models are coded according to the symbol and numerical values of design parameters. For example; ST-1-0.87-1-5: in the case of the stair damper design, taking into account the 1st mode response, the period ratio of 0.87, limit damping coefficient of 1×10^6 Nsec/m and the allowable relative displacement of 5 cm are coded. For only 2 stair models selected, the change of the objective function during numerical optimization is shown for both modes in Fig. 13. These graphs show the status during the numerical optimization in the last step of the proposed algorithm. When the added damping ratio is 9%, optimum design is achieved in both the first and second modes. The convergence can also be clearly seen here. The convergence for Nelder Mead method is providing in the last steps and suddenly in Fig. 13(a). This is related to the working principle of the Nelder Mead algorithm. Algorithm is able to reach the optimum solution with vertical changes, and after the optimum is attained, Nelder Mead Algorithm is stopped. The sudden changes of the objective function in the vertical axis can also be seen more clearly by changing the setting parameters of the Nelder Mead method.

The upper limit of the damping coefficient is fixed at

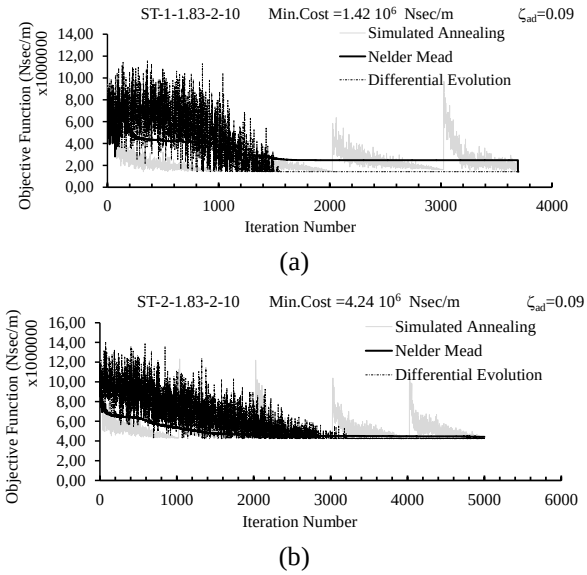

Fig. 13 The variation of the objective function according to the iteration number in numerical optimization for three numerical optimization methods in case of (a) Mode 1 and (b) Mode 2 in stair model

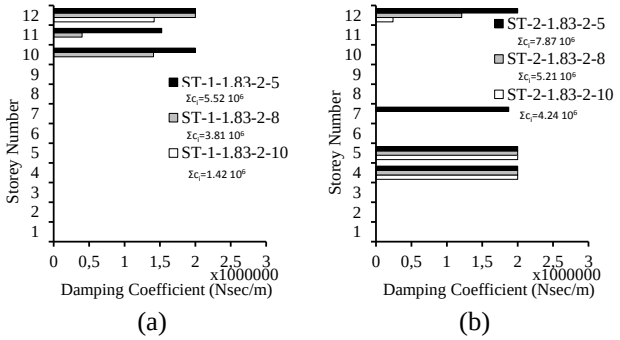

Fig. 14 Optimum distribution of damping coefficients for the change of $\overline{RD}$ in case of (a) Mode 1and (b) Mode 2 in stair model

$\bar{c}_i = 2 \times 10^6$ Nsec/m, the period ratio is taken as 1.83 and the allowable limit values of the relative displacement are selected as $\overline{RD}$=5 cm; 8 cm; 10 cm. As the $\overline{RD}$ limit allowable value decreases both the number of storey to which the dampers are added and the total damper amount increases, as shown in Fig. 14(a) when the first mode is taken into account. In case of $\overline{RD}$=10 cm, only the minimum amount of damper placement on the top floor is sufficient. When the second mode behavior is considered, it is observed that the top and middle storeys are the critical zones to prevent the collision (Fig. 14(b)). As the $\overline{RD}$ increases, the optimum damper amount and location number are reduced. If the effect of the mode behavior is compared, the dampers are placed less storeys and less dampers are needed in the first mode in Fig. 14(a).

When the models ST-1-1.83-2-10 and ST-2-1.83-2-10 are chosen in Fig. 14, it is observed in Fig. 15 that all RD values are reduced below the allowable level for both modes. The added damping ratio attain to 8% in both the first and second mode control. As can be seen from Fig. 16, the RD

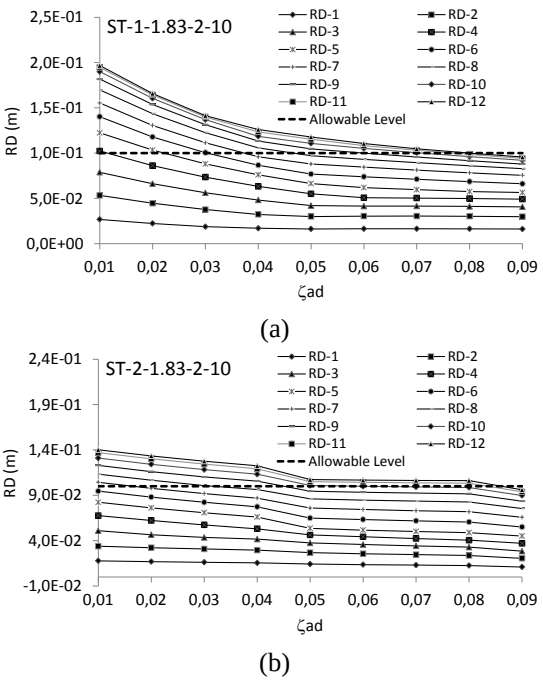

Fig. 15 The variation of relative displacements according to added damping ratio in case of (a) Mode 1 and (b) Mode 2 in stair model

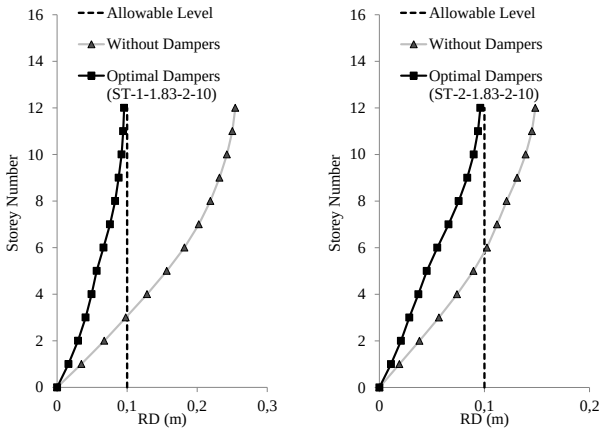

Fig. 16 Peak relative displacement values for optimal damper design in case of (a) Mode 1 and (b) Mode 2 in stair model

values of without damper models exceed the allowable relative displacement in the floor levels. It is displayed that the peak relative displacements at all storeys are attained below the desired level.

Considering the first and second mode behaviors, the effect of the limit of the damping coefficient ($\bar{c}_i$) on the optimum damping allocation is seen in Fig. 17. If the damper designs found by taking the first mode behavior are examined, the reduction of $\bar{c}_i$ increases both the total amount of damper and the number of floors in which the dampers are placed, as can be seen from Fig. 17(a). If the second mode is regarded for optimization, the dampers are focused to the middle storeys where is the critical region in terms of collision. The dampers have reached the limit values

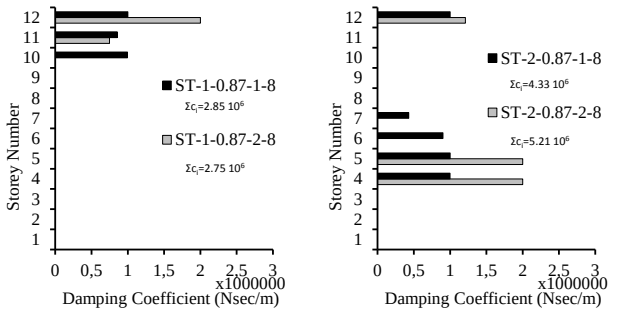

Fig. 17 Optimum distribution of damping coefficients for the change of $\bar{c}_i$ in case of (a) Mode 1 and (b) Mode 2 in stair model

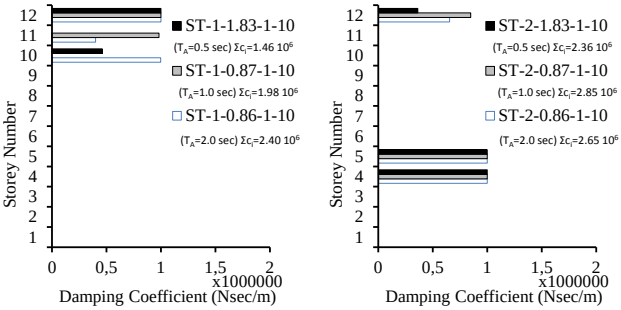

Fig. 18 Optimum distribution of damping coefficients for the change of T_B/T_A in case of (a) Mode 1 and (b) Mode 2 in stair model

in these regions and then settled on the upper floors which are the other critical region as shown in Fig. 17(b). The increase of $\bar{c}_i$ decrease the location of dampers, while the total amount of dampers increase. If the optimal damper designs made according to the second mode are compared with the optimum designs according to the first mode, a greater amount of damper and more damper locations are observed in the second mode.

In the first mode, the general trend in the damper distributions is expected to be placed downward from the top floor of the structure, while it is placed on the 12th storey and then it is located to the 10th storey in the model with T_A=0.5 sec When T_A=1.0 sec, the dampers are placed on the 11th and 12th storeys, when T_A is equal 2.0 sec, the dampers are distributed to the 10th, 11th and 12th floors as shown in Fig. 18(a). In this case, the small amount of damper is placed on the 11th floor. As can be seen from this figure, the increase in the period of structure A also increases the total amount of damper added. Fig. 18(b) shows the optimum damper distribution corresponding to the second mode. There is no change in the storeys on which the dampers are placed with T_A change. In terms of the amount of damper coefficients placed on the storeys, there is no significant difference between them. If the optimum designs according to the second mode are compared with the optimum designs according to the first mode, both the number of damper location and the total damper amount in the model structures are increased.

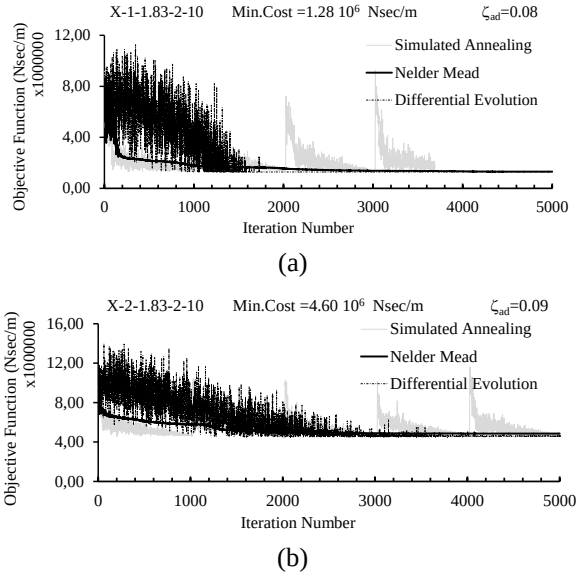

Fig. 19 The variation of the objective function according to the iteration number in numerical optimization for three numerical optimization methods in case of (a) Mode 1 and (b) Mode 2 in *X*-diagonal model

5.3 X-Diagonal model

In the *X*-diagonal models designed as shown in Fig. 6(c), the dampers are placed in the *X*-shape between sequential storeys. The total damping coefficient value in a storey considered is the sum of the damping coefficients of the two dampers on that floor. In this section, the same analyzes are made for *X*-diagonal models and their results are discussed in a similar way to analyzes in the sections where classical and stair damper designs are applied. The *X*-diagonal damper models are coded with the symbol and numerical values of the design parameters. For example; X-2-0.86-1-10: *X* denotes *X*-diagonal damper design, second term (2) is the number of mode, the third term (0.86) presents the period ratio, fourth term (1×10^6 Nsec/m) is the limit damping coefficient and the last term (10 cm) is defined as allowable relative displacement. Fig. 19 shows the change of the objective function during the three different numerical optimization processes and the convergence of the optimization as a result of the optimal design phase of the two *X*-diagonal models for the first two modes. Three different optimization methods achieve the same optimum values and their results confirm each other.

In the case of the *X*-diagonal dampers inserted between adjacent structures to prevent pounding, the number of damper locations optimally placed decreases as the amount of relative displacement allowed increases in the first mode (Fig. 20(a)). In the same way, the total amount of damper added in the building decreases. Moreover, in the first mode, the dampers concentrate on the top region of the structure. According to the second mode case, Fig. 20(b) is examined; the optimal damper placement is seen as the middle floors (4th, 5th and 6th floors) and the top storeys (11th and 12th) for all $\overline{RD}$ cases. In the case of $\overline{RD}$=8 cm and 10 cm, the same optimum designs are achieved on the middle storeys, the

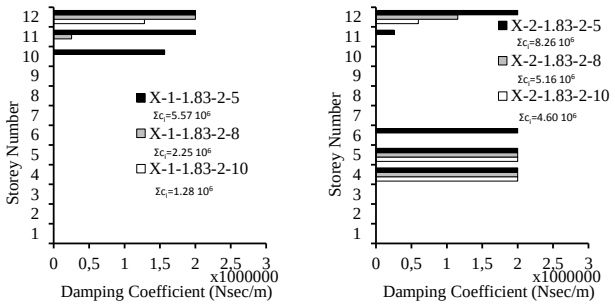

(a) (b)

Fig. 20 Optimum distribution of damping coefficients for the change of $\overline{RD}$ in case of (a) Mode 1and (b) Mode 2 in *X*-diagonal model

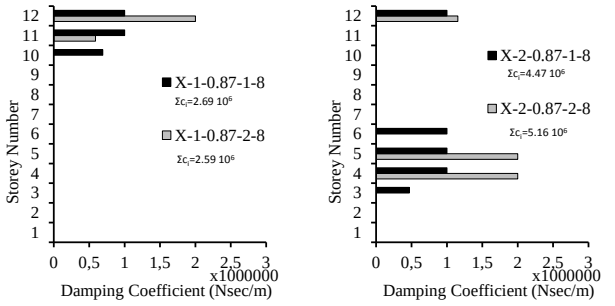

(a) (b)

Fig. 21 Optimum distribution of damping coefficients for the change of $\bar{c}_i$ in case of (a) Mode 1 and (b) Mode 2 in *X*-diagonal model

optimum damper coefficient at top storey for $\overline{RD}$=5 cm reaches a larger damper than the other two design. As with the first mode control, the increase of $\overline{RD}$ in the control of the second mode reduces the total damper amount. The dampers are concentrated to middle storeys with large quantities and top storey with little quantities in the second mode, while it focuses on top storeys in the first mode.

The effect of the variation of the upper limit of the damping coefficient in the damper distribution is inquired in Fig. 21 for the *X*-diagonal damper models. In the first mode, both the number of damper locations and the total damper amount decrease with increase of the upper limit of the damper in Fig. 21(a). In this case, the dampers also focus on the upper floors. In the second mode control as shown in Fig. 21(b), there is important decrement in the number of damper locations with the increase of the upper limit, while the total amount of optimal damping coefficient used increases significantly. Dampers are predominantly distributed to the middle floors while they are added to the top floor. The more locations and amounts of damper are placed in the second mode according to the first mode.

The models X-1-1.83-2-10 and X-2-1.83-2-10 are selected in Fig. 21 to prove the reduction below the allowable level of RD for all relative displacement in Fig. 22. Fig. 22(a) shows the variation of the RDs in the first mode and Fig. 22(b) in the second mode with respect to the added damping ratio. In the first mode, when the added damping ratio of 8% is reached, the optimum design is achieved by reducing the target below the RD value, while the optimal

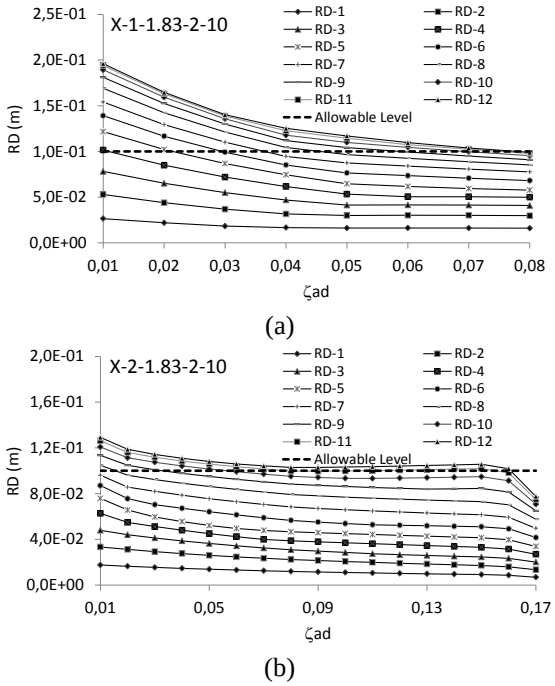

(a)

(b)

Fig. 22 The variation of relative displacements according to added damping ratio in case of (a) Mode 1 and (b) Mode 2 in *X*-diagonal model

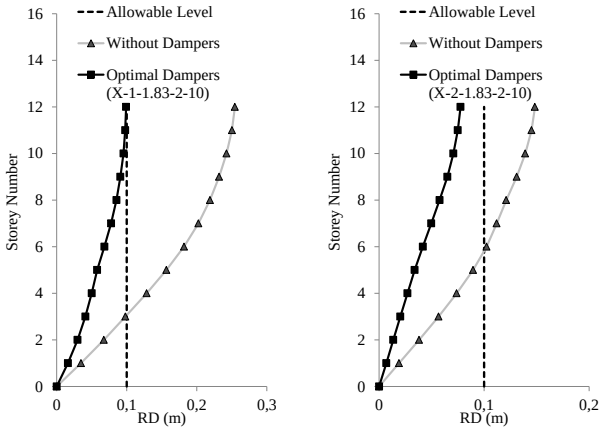

(a) (b)

Fig. 23 Peak relative displacement values for optimal damper design in case of (a) Mode 1 and (b) Mode 2 in *X*-diagonal model

design is obtained by reaching the damping ratio 9% in the second mode. In the without dampers cases, the risk of collision will occur as the relative displacements exceed the permissible limit relative displacement as seen from the Fig. 23. It is clear that the calculated relative displacements at the floor levels are reduced below the desired relative displacement limit for both modes.

Fig. 24 shows the damper distribution according to the variation the period of structure A for both modes. When Fig. 24(a) is examined, it is seen that with the increase of T_A value, the total amount of damping coefficient increase. In the case of T_A=0.5 sec and T_A=1.0 sec, the number of locations is the same, whereas in T_A=2.0 sec, the number of locations increases. Because the increase in the value of the

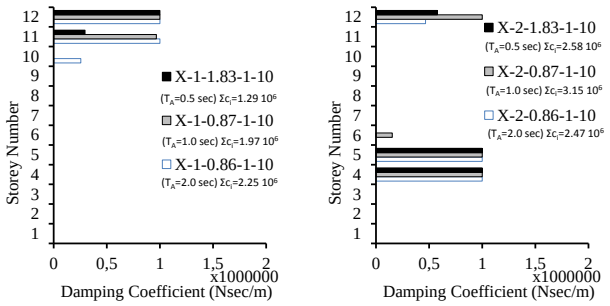

Fig. 24 Optimum distribution of damping coefficients for the change of T_B/T_A in case of (a) Mode 1 and (b) Mode 2 in *X*-diagonal model

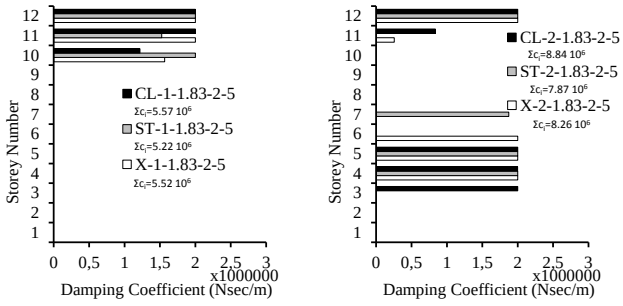

Fig. 25 Optimum distribution of damping coefficients for the change of damper design type in case of (a) Mode 1 (b) Mode 2

T_A causes larger relative displacements between the buildings and this leads to the need for more dampers. If the change of the damper distribution according to the second mode with the T_A is examined in Fig. 24(b), the same location number is obtained for the cases where the T_A is 0.5 sec and 2 sec. In case of T_A=1.0 sec, more number of locations is reached. In the case of T_A=0.5 sec and 2 sec, the total amount of damper is close, while in the case of T_A=1.0 sec this amount is increased. When the mode effect on the damper distribution is considered, it is seen that in the design obtained for the second mode control, the damper is added in more amount and in more locations than in the first mode. Although there is a high risk zone for collision at the top storey, the second mode control has a high risk of collision in the middle floors. This leads to the need for more the total amount and location of dampers.

5.4 Comparison of damper design types

In the previous parts of the numerical example, three different types of damper designs are examined separately. In this section, optimum designs are compared for three different model types (Classical, Stair and *X*-diagonal model) for the same mode cases, period ratio, upper limit of the damping coefficient and the allowable relative displacement. The optimal placement for three different damper designs made according to the first mode is given in Fig. 25(a). The optimal dampers are focused to the upper storeys in the first mode control for all design types. When

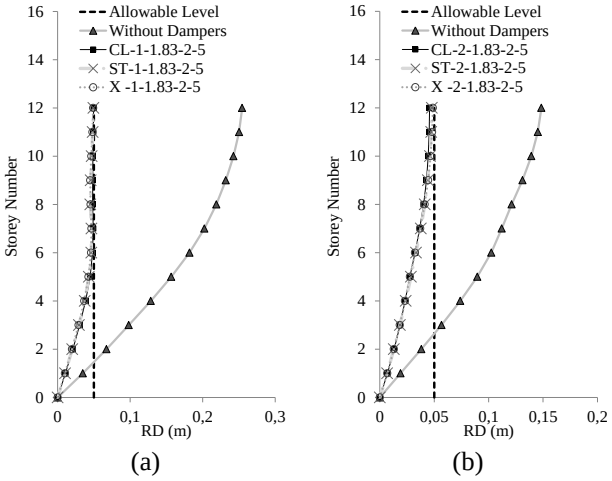

Fig. 26 Peak relative displacement values for different types of damper designs in case of (a) Mode 1 and (b) Mode 2

the locations of dampers are examined, it shows the same places in three designs. Three different damper designs types are observed to be close to each other according to total damper quantities. However, while the best design between these three designs is stair design, the other two are quite close to each other. In the second mode control as shown in Fig. 25(b), dampers for all designs are placed on the 4th, 5th and 12th floors, while dampers are also added to the 3rd and 11th floors for classical design, to the 7th floor for stair design and to the 11th floor for the diagonal design. In the case of the control of both modes, it is seen that the best is the stair design and the worst is the classic design in terms of the total amount of damping

In the case of the control of both the first and second modes in Fig. 26, the results of the three different types of damper design are shown in the profile of the relative displacements of the storey level under the earthquake effect.

6. Conclusions

The major contributions of this study encompass (1) to propose the algorithm for optimum placement of viscous dampers in order to prevent collision between two adjacent buildings; (2) to investigate and determine the critical period ratios via the relative displacement spectra; (3) to demonstrate the algorithm through the applications of the two adjacent 12-story buildings with three viscous damper configurations such as classical, stair and *X*-diagonal configurations.

An algorithm is proposed that minimizes the sum of the damping coefficients of the dampers to reach a target modal damping ratio and to attain below an allowable relative displacement limit under a design earthquake loads. Differences in periods of adjacent structures are known to cause out of phase behavior of buildings. In this case, the risk of structural pounding at which critical period ratios can occur is examined and a new relative displacement spectrum is developed for a design earthquake to determine these critical period ratios. By using critical period ratios at points where the relative displacement spectrum reaches peak

values, numerical models are constructed for the worst scenario in terms of collision risk.

In order to prevent the structural collision, the parameters on the optimum damper distribution problem are also examined. Twelve-storey adjacent building models are selected as a numerical example, and the proposed method is tested. The effects of damper design type, the allowable relative displacement, the period ratios of adjacent buildings, the upper limit of each damper placed on the storeys and the mod behavior of the structure on optimum damper allocation and the structural response are investigated in detail. The results of the numerical analysis are summarized below:

- Using the El Centro (NS) earthquake acceleration record, the relative displacement spectrum for the two adjacent building structure models, each with a single degree of freedom, is plotted for primary building periods as T_A=0.5 sec, 1.0 sec and 2.0 sec. In case T_A is 0.5 sec, 1.0 sec and 2.0 sec, the critical period ratios are obtained from the new spectrum as 1.83, 0.87 and 0.86. These critical period ratios are used to arrange the numerical models.
- Considering the first mode of the primary structure, while the dampers concentrate on the top floors, while the second mode is regarded, they are distributed to both the middle floors and the top floors.
- In all types of damper design, the total amount of damping coefficient corresponding to the designs in the second mode is higher than in the first mode. Furthermore, there is a need to place more locations of damper and more total damping amount to control the second mode.
- The increase in the allowable relative displacement value results in a lower total amount of damping and less location of damper in all models.
- At the end of all the optimal designs found, relative displacements at all storey levels under the design earthquake are verified by decreasing below the $\overline{RD}$.
- When all models are examined for both mode controls, the increase in the upper limit of the damper at each storey decreases the number of dampers added.
- When the first mode is taken into account, the increase in the upper limit of the damper increases the total amount of damping in the classical design, whereas in the stair and X-diagonal design it decreases. When the same issue is examined for the second mode, the increase in the upper limit value in the classical design leads to a decrease in total damping, whereas in stairs and X-diagonal design the increase is observed in total damping amount.
- In designs according to the first mode, the increase in the primary structural period (T_A) increases the total damper amount, while in the case of T_A=0.5 sec and T_A=1.0 sec there is an equal damper locations, but in case of T_A=2.0 sec the number of locations increases. In the designs according to the second mode, an equal number of dampers are added in the case of T_A=0.5 sec and T_A=2 sec, whereas in T_A=1.0 sec the number of locations are increased. According to the second mode, an approximate total damping amount are found to be similar for the case of T_A=0.5 sec and T_A=2 sec, while it is increased in T_A=1.0 sec.
- When a comparison is made between the distributions of the three different damper design types in the first mode, the location numbers and the storeys placed of dampers are the same. However, the total damping amounts are very close to each other optimal designs. When the second mode is considered for designing of the dampers, the location numbers of the added dampers and total damping amounts obtained are close to each other optimal design, while there are some differences in the settlements between three different types of dampers designs.
- All optimum designs are compatible with each other and below the allowable level to prevent the structural pounding.

Analyses find out that the proposed method offers the designers optimum distribution of viscous dampers to minimize the risk of pounding of adjacent structures during the earthquake according to the application of various types of dampers.

References

Abdeddaim, M., Ounis, A., Djedoui, N. and Shrimali, M.K. (2016), "Pounding hazard mitigation between adjacent planar buildings using coupling strategy", *Struct. Control Hlth. Monit.*, **6**, 603-617.

Abdullah, M.M., Hanif, J.H., Richardson, A. and Sobanjo, J. (2001), "Use of a shared tuned mass damper (STMD) to reduce vibration and pounding in adjacent structures", *Earthq. Eng. Struct. Dyn.*, **30**, 1185-1201.

Aldemir, U. and Aydin, E. (2005), "An active control algorithm to prevent the pounding of adjacent structures", *Vib. Prob. ICOVP*, 33-38.

Amini, F. and Ghaderi, P. (2013), "Hybridization of harmony search and ant colony optimization for optimal locating of structural dampers", *Appl. Soft. Comput.*, **13**, 2272-2280.

Anagnostopoulos, S.A. (1995), "Earthquake induced pounding: state of the art", *Proceedings of the 10th Europ. Conf. on Earth. Eng.*, 897-905.

Aydin, E. (2013), "A simple damper optimization algorithm for both target added damping ratio and interstorey drift ratio", *Earthq. Struct.*, **5**(1), 083-109.

Aydin, E., Boduroglu, M.H. and Guney, D. (2007), "Optimal damper distribution for seismic rehabilitation of planar building structures", *Eng. Struct.*, **29**, 176-185.

Basili, M. and De Angelis, M. (2007), "Optimal passive control of adjacent structures interconnected with nonlinear hysteretic devices", *J. Sound Vib.*, **301**, 106-125.

Bekdas, G. and Nigdeli, S.M. (2012), "Preventing the pounding of adjacent buildings with harmony search optimized tuned mass damper", *3rd Euro. Conf. of Civ. Eng.*, Paris, France.

Bharti, S.D., Dumne, S.M. and Shrimali, M.K. (2010), "Seismic response analysis of adjacent buildings connected with MR dampers", *Eng. Struct.*, **32**, 2122-2133.

Bhaskararao, A.V. and Jangid, R.S. (2006), "Seismic response of adjacent buildings connected with friction dampers", *Bull. Earthq. Eng.*, **4**(1), 43-64.

Bigdeli, K., Hare, W. and Tesfamariam, S. (2012), "Configuration optimization of dampers for adjacent buildings under seismic excitations", *Eng. Optim.*, **44**(12), 1491-1509.

Chau, K.T., Wei, X.X., Guo, X. and Shen, C.Y. (2003), "Experimental and theoretical simulations of seismic poundings

between two adjacent structures", *Earthq. Eng. Struct. Dyn.*, **32**, 537-554.
Chouw, N. and Hao, H. (2012), "Pounding damage to buildings and bridges in the 22 February 2011 Christchurch earthquake", *Int. J. Protec. Struct.*, **3**(2), 123-139.
Cundumi, O. and Suarez, L.E. (2008), "Numerical investigation of a variable damping semiactive device for the mitigation of the seismic response of adjacent structures", *Comput. Aid. Civil Infrastr. Eng.*, **23**, 291-308.
Garcia, D.L. and Soong, T.T. (2009), "Assessment of the separation necessary to prevent seismic pounding between linear structural systems", *Prob. Eng. Mech.*, **24**, 210-223.
Hameed, A., Saleem, M., Qazi, A.U., Saeed, S. and Bashir, M.A. (2012), "Mitigation of seismic pounding between adjacent buildings", *Pak. J. Sci.*, **64**(4), 326-333.
Hameed, M., Tsuji, M. and Takewaki, I. (2013), "Smart passive control of buildings with higher redundancy and robustness using base-isolation and inter-connection", *Earthq. Struct.*, **4**(6), 649-670.
Hong, H.P., Wang, S.S. and Hong, P. (2003), "Critical building separation distance in reducing pounding risk under earthquake excitation", *Struct. Saf.*, **25**, 287-303.
Jankowski, R. (2008), "Earthquake-induced pounding between equal height buildings with substantially different dynamic properties", *Eng. Struct.*, **30**(10), 2818-2829.
Jankowski, R. and Mahmoud, S. (2015), *Earthquake-Induced Structural Pounding*, Springer, Switzerland.
Jeng, V., Kasai, K. and Maison, B.F. (1992), "A spectral difference method to estimate building separations to avoid pounding", *Earthq. Spectra*, **8**(2), 201-223.
Karayannis, C.G. and Favvata, M.J. (2005), "Earthquake-induced interaction between adjacent reinforced concrete structures with non-equal heights", *Earthq. Eng. Struct. Dyn.*, **34**(1), 1-20.
Khatiwada, S., Chouw, N. and Butterworth, J.W. (2014), "A generic structural pounding model using numerically exact displacement proportional damping", *Eng. Struct.*, **62-63**, 33-41.
Kim, J., Ryu, J. and Chung, L. (2006), "Seismic performance of structures connected by viscoelastic dampers", *Eng. Struct.*, **28**, 183-195.
Komodromos, P. (2008), "Simulation of the earthquake-induced pounding of seismically isolated buildings", *Comput. Struct.*, **86**, 618-626.
Lin, J.H. (1997), "Separation distance to avoid seismic pounding of adjacent buildings", *Earthq. Eng. Struct. Dyn.*, **26**(3), 395-403.
Lin, J.H. and Weng, C.C. (2001), "Probability analysis of seismic pounding adjacent buildings", *Earthq. Eng. Struct. Dyn.*, **30**(10), 1539-1557.
Luco, J.E. and De Barros, F.C.P. (1998), "Optimal damping between two adjacent elastic structures", *Earthq. Eng. Struct. Dyn.*, **27**, 649-659.
Mahmoud, S., Chen, X. and Jankowski, R. (2008), "Structural pounding models with hertz spring and nonlinear damper", *J. App. Sci.*, **8**(10), 1850-1858.
Matsagar, V.A. and Jangid, R.S. (2005), "Viscoelastic damper connected to adjacent structures involving seismic isolation", *J. Civil Eng. Manage.*, **11**(4), 309-322.
Mazanoglu, E.C.K. and Mazanoglu, K. (2017), "An optimization study for viscous dampers between adjacent buildings", *Mech. Syst. Signal Pr.*, **89**, 88-96.
Mouzakis, H.P. and Papadrakakis, M. (2004), "Three dimensional nonlinear building pounding with friction during earthquakes", *J. Earthq. Eng.*, **8**(1), 107-132.
Muthukumar, S. and DesRoches, R. (2006), "A Hertz contact model with non-linear damping for pounding simulation", *Earthq. Eng. Struct. Dyn.*, **35**, 811-828.
Park, K.S. and Ok, S.Y. (2015), "Hybrid control approach for seismic coupling of two similar adjacent structures", *J. Sound Vib.*, **349**, 1-17.
Patel, C.C. and Jangid, R.S. (2010), "Seismic response of dynamically similar adjacent structures connected with viscous dampers", *IES J. Part A: Civil Struct. Eng.*, **3**(1), 1-13.
Patel, C.C. and Jangid, R.S. (2014), "Dynamic response of identical adjacent structures connected by viscous damper", *Struct. Control Hlth. Monit.*, **21**, 205-224.
Penzien, J. (1997), "Evaluation of building separation distance required to prevent pounding during strong earthquakes", *Earthq. Eng. Struct. Dyn.*, **26**(8), 849-858.
Polycarpou, P.C. and Komodromos, P. (2010), "Earthquake-induced poundings of a seismically isolated building with adjacent structures", *Eng. Struct.*, **32**, 1937-1951.
Quinonero, F.P., Massegu, J.R., Rossell, J.M. and Karimi, H.R. (2012), "Semiactive-passive structural vibration control strategy for adjacent structures under seismic excitation", *J. Frank. Inst.*, **349**, 3003-3026.
Quinonero, F.P., Massegu, J.R., Rossell, J.M. and Karimi, H.R. (2014), "Vibration control for adjacent structures using local state information", *Mechatron.*, **24**, 336-344.
Raheem, S.E.A. (2006), "Seismic pounding between adjacent building structures", *Electr. J. Struct. Eng.*, **6**, 66-74.
Rajaram, C. and Kumar, R.P. (2015), "Calculation of separation distance between adjacent buildings: a review on codal provisions", *J. Seismol. Earthq. Eng.*, **17**(1), 31-42.
Rosenblueth, E. and Meli, R. (1986), "The 1985 earthquake: causes and effects in Mexico City", *Concrete Int.*, **8**(5), 23-34.
Schexnayder, C., Alarcon, L.F., Antillo, E.D., Morales, B.C. and Lopez, M. (2014), "Observations on bridge performance during the Chilean earthquake of 2010", *J. Constr. Eng. Manage.*, **140**(4), B4013001-1-6.
Shakya, K. and Wijeyewickrema, A.C. (2009), "Mid-column pounding of multi-story reinforced concrete buildings considering soil effects", *Adv. Struct. Eng.*, **12**(1), 71-85.
Soltysik, B., Falborski, T. and Jankowski, R. (2017), "Preventing of earthquake-induced pounding between steel structures by using polymer elements: experimental study", *Proc. Eng.*, **199**, 278-283.
Sonmez, M., Aydin, E. and Karabork, T. (2013), "Using an artificial bee colony algorithm for the optimal placement of viscous dampers in planar building frames", *Struct. Multi. Optim.*, **48**, 395-409.
Stavroulakis, G.E. and Abdalla, K.M. (1991), "Contact between adjacent structures", *J. Struct. Eng.*, **117**(10), 2838-2850.
Takewaki, I. (1997), "Optimal damper placement for minimum transfer functions", *Earthq. Eng. Struct. Dyn.*, **26**, 1113-1124.
Takewaki, I. (2000), "Optimal damper placement for planar building frames using transfer functions", *Struct. Multi. Optim.*, **20**, 280-287.
Tubaldi, E., Barbato, M. and Ghazizadeh, S. (2012), "A probabilistic performance-based risk assessment approach for seismic pounding with efficient application to linear systems", *Struct. Saf.*, **36-37**, 14-22.
Turkish Building Earthquake Code (2019), Prime Ministry, Disaster and Emergency Management Presidency, AFAD, Turkey.
Uz, M.E. and Hadi, M.N.S. (2014), "Optimal design of semi active control for adjacent buildings connected by MR damper based on integrated fuzzy logic and multi-objective genetic algorithm", *Eng. Struct.*, **69**, 135-148.
Valles-Mattox, V.E. and Reinhorn, A.M. (1996), "Evaluation, prevention and mitigation of pounding effects in building structures", *Eleven. World Conf. Earthq. Eng.*, Paper No. 26.
Wolfram Research (2003), Mathematica Edition Version 5.0, Wolfram Research, Champaign, Illinois.
Xu, Y.L. and Zhang, W.S. (2002), "Closed-form solution for seismic response of adjacent buildings with linear quadratic

Gaussian controllers", *Earthq. Eng. Struct. Dyn.*, **31**, 235-259.
Xu, Y.L., He, Q. and Ko, J.M. (1999), "Dynamic response of damper-connected adjacent buildings under earthquake excitation", *Eng. Struct*., **21**,135-148.
Yang, Z., Xu, Y.L. and Lu, X.L. (2003), "Experimental seismic study of adjacent buildings with fluid dampers", *J. Struct. Eng.*, **129**(2), 197-205.
Ying, Z.G., Ni, Y.Q. and Ko, J.M. (2003), "Stochastic optimal coupling-control of adjacent building structures", *Comput. Struct.*, **81**, 2775-2787.
Yu, Z.W., Liu, H.Y., Guo, W. and Liu, Q. (2017), "A general spectral difference method for calculating the minimum safety distance to avoid the pounding of adjacent structures during earthquakes", *Eng. Struct.*, **150**, 646-655.
Zhang, W.S. and Xu, Y.L. (1999), "Dynamic characteristics and seismic response of adjacent buildings linked by discrete dampers", *Earthq. Eng. Struct. Dyn*., **28**(10),1163-1185.
Zhu, H., Wen, Y. and Iemura, H. (2001), "A study on interaction control for seismic response of parallel structures", *Comput. Struct.*, **79**, 231-242.
Zhu, H.P. and Xu, Y.L. (2005), "Optimum parameters of Maxwell model defined damper used to link adjacent structures", *J. Sound Vib.*, **279**, 253-274.
Zhu, H.P., Ge, D.D. and Huang, X. (2011), "Optimum connecting dampers to reduce the seismic responses of parallel structures", *J. Sound Vib.*, **330**, 1931-1949.

KT